AIAA 2003-0746

A Computational Study of the Abrupt Wing Stall (AWS) Characteristics for Various Fighter Jets: Part I, F/A-18E and F-16C

Paresh Parikh
NASA Langley Research Center, Hampton, VA

James Chung
Naval Air Systems Command, Patuxent River, MD

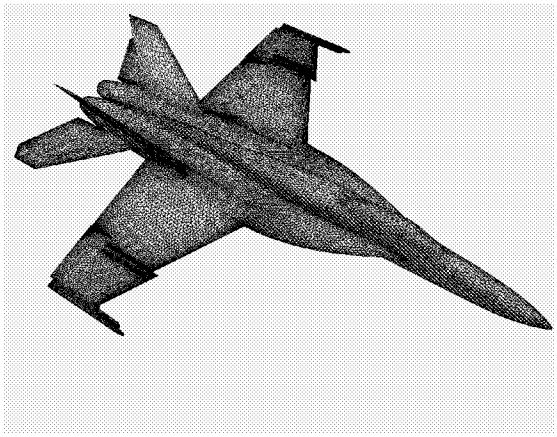

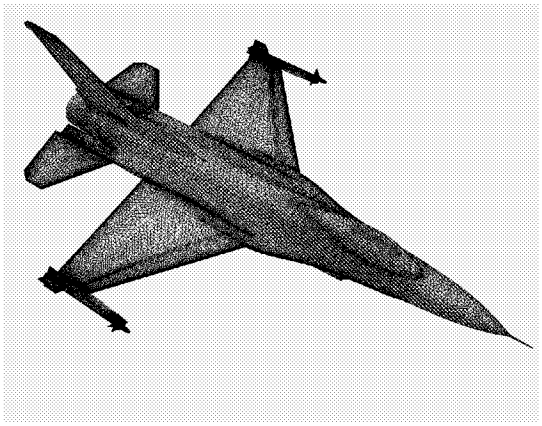

41st Aerospace Sciences Meeting and Exhibit
January 6-9, 2003
Reno, Nevada

AIAA-2003-0746

A Computational Study of the Abrupt Wing Stall (AWS) Characteristics for Various Fighter Jets: Part I, F/A-18E and F-16C

Paresh Parikh*
NASA Langley Research Center, Hampton, VA

James Chung†
Naval Air Systems Command, Patuxent River, MD

ABSTRACT

Steady state Computational Fluid Dynamic (CFD) simulations are used to gain an understanding of the physics behind the Abrupt Wing Stall (AWS) phenomenon and to arrive at static Figures of Merit (FOMs). Navier-Stokes simulations are conducted using the NASA Langley developed TetrUSS simulation suite which is based on tetrahedral, unstructured grids. The physics of the AWS phenomenon is understood by comparing CFD simulation results on two aircraft; a pre-production F/A-18E configuration which exhibits AWS phenomenon under certain geometric and flow conditions, and an F-16C aircraft configuration that does not. The CFD code is first validated against two sets of experimental data to build confidence in its use for the problem of AWS. An attempt is then made to understand the possible causes of AWS by analyzing and comparing the detailed flow fields between the two configurations under a variety of flow conditions. Based on this approach, a number of static Figures of Merit are developed to predict the potential existence of AWS. The FOMs include the break in the lift and wing root bending moment versus angle-of-attack (AoA) curves and the rate of change of sectional lift with respect to AoA. A companion paper, in Part II, describes a similar CFD study on two other aircraft, the AV-8B Harrier and F/A-18C. Results from both these studies, as well as other CFD studies conducted as part of the AWS program are used to recommend a CFD procedure for predicting the existence of AWS in future aerospace designs.

INTRODUCTION

Abrupt Wing Stall (AWS) is the uncommanded lateral-directional motion experienced by an aircraft during transonic maneuvering conditions. One of the aims of the joint NASA/Navy/AF AWS Program was to understand the physical flow mechanism responsible for the phenomenon. Such an understanding can then be used to arrive at guidelines with which to evaluate any new aerospace design for the likelihood of AWS and if found, to fix the problem in the early design phase.

The program contained an extensive and complementary combination of experimental and computational studies; both steady and unsteady, to accomplish this aim. These studies were designed to learn the physics behind the AWS phenomenon by comparing and contrasting data on configurations that did and did not show AWS tendencies in flight. The aircraft configurations studied included a pre-production F/A-18E and AV-8B, both showing AWS when flown at a certain combination of geometric and flow conditions. Results on these were compared with similar results for the F-16C and F/A-18C, both of which do not exhibit AWS in their normal operational regime.

The present study is the first of a two-part CFD study complementing the static wind-tunnel tests conducted during the AWS program. Each part compares and contrasts one aircraft configuration that exhibits AWS and one that does not. Both of these studies were conducted using a high-fidelity, unstructured-grid based Navier-Stokes solver. This paper, Part I, presents the results for the F/A-18E and F-16C

*Senior Research Engineer, Associate Fellow AIAA.

†Aerospace Engineer, Senior Member AIAA

configurations. Part II[1] presents similar results for the AV-8B and F/A-18C aircraft configurations.

The objectives of the present study are first listed, followed by a description of the computational method used, as well as its validation. An analysis of the computational results is then presented, and a set of Figures of Merit (FOMs) are developed against which to measure future aircraft configurations. Finally, important conclusions from the study are presented.

OBJECTIVES OF THE STUDY

The first objective of the present study was to develop a validated CFD procedure, based on existing unstructured grid-based steady state CFD technology, for evaluating aircraft designs for AWS. The second objective was to analyze the underlying flow physics that may be responsible for AWS. The final aim was to arrive at static Figures of Merit as well as recommendations which may be used to screen future aircraft designs for AWS.

COMPUTATIONAL METHOD

All the computations presented in this paper were carried out using the NASA Langley developed TetrUSS suite of codes. TetrUSS[2] is a complete flow analysis system based on unstructured, tetrahedral grids. The Navier-Stokes grids were generated and grid quality improvements accomplished using the component codes VGRIDns[3] and POSTGRIDns, respectively.

The flow solutions were obtained using the TetrUSS flow solver component, USM3Dns[4]. This is a three dimensional, tetrahedral, cell-centered, finite-volume, Euler and Navier-Stokes flow solver. In USM3Dns, the inviscid flux quantities are computed across each cell face using Roe's flux difference splitting (FDS). Spatial discretization is accomplished by a novel reconstruction process, which is based on an analytical formulation for computing solution gradients within tetrahedral cells. The solution is advanced to a steady state condition by an implicit backward-Euler time-stepping scheme. Flow turbulence effects are modeled by the Spalart-Allmaras one equation model. USM3Dns can be run in either a full viscous or a wall-functions mode. However, all the calculations in the present study were performed using the full viscous mode.

USM3Dns runs on massively parallel computers and on clusters of personal computers. Although a single processor version is available for a variety of computing platforms, the parallel version[5] is the code of choice because it enables rapid turn-around for large problems.

Aircraft Configurations:

Two aircraft configurations were selected for examination related to AWS for this study: A pre-production F/A-18E configuration which showed AWS tendencies during early flight tests and an F-16C configuration that exhibited no AWS tendencies in its normal operational region. Since the CFD code was calibrated using experimental data, an attempt was made to closely reproduce as many of the geometric details of the wind-tunnel test model as practical including the wing tip missile and its attachment hardware as well as flow through ducts representing the engine flow path. Only one side of the symmetric aircraft configuration was modeled, utilizing a plane-of-symmetry boundary condition along the aircraft centerline. The grid resolution used in the CFD study was sufficient to provide a grid spacing of $y^+=1$ right next to the body surface based on the wind-tunnel test Reynolds number.

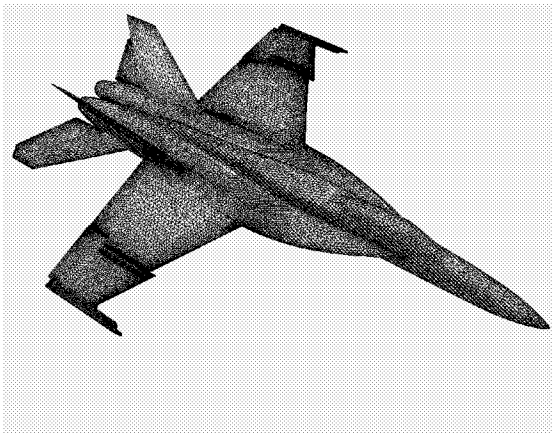

F/A-18E

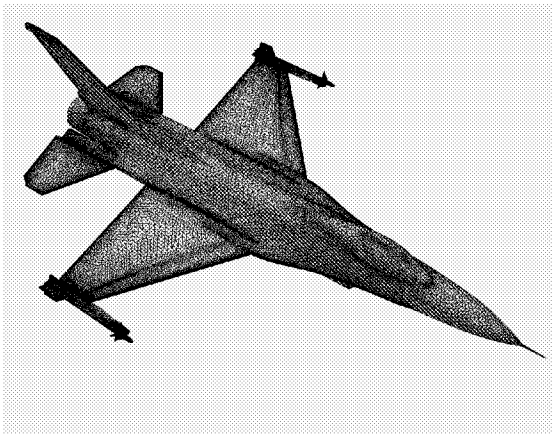

F-16C

Figure 1: Surface grid for F/A-18E and F-16C configurations.

The F/A-18E configuration had a flap setting of $10^{o}/10^{o}/5^{o}$ - LE/TE/Aileron deflections, respectively, and has been designated as F/A-18E, 10/10/5 in this paper. The unstructured, viscous grid consisted of 3,786,448 tetrahedral cells and 654,840 points. The F-16C configuration modeled has a designation of Block 25 to distinguish it from other configurations of the same airplane with small geometrical differences. The configuration had 0^{o} deflections for both the LE and TE flaps. The grid had 6,929,816 tetrahedral cells and 1,205,202 points.

Figure 1 shows triangulated surfaces for both configurations. Although the full aircraft configurations are shown in the picture, the CFD study used only half-span configurations, as previously stated.

Calibration of the Computer Code:

The unstructured grid-based N-S solver, USM3Dns, was first calibrated by comparing the CFD force and moment data against wind-tunnel results obtained during companion studies of the AWS program. For the F-16C, Block 25 configuration, the CFD data were compared against Veridian (formerly CALSPAN) 8-FT transonic tunnel test T05-590 and NASA Langley Research Center (LaRC) 16-FT Transonic wind-tunnel tests. The comparisons were made for a free-stream Mach number of 0.8 at a series of angles-of-attack (AoA) from 6.0^{0} to 16.0^{0}. Although the two tests were run at slightly different unit Reynolds number (Reynolds number per foot of 2.5×10^{6} for the Veridian test versus 3.63×10^{6} for the LaRC test), the CFD was run to match that of the Veridian data. The parallel version of USM3Dns was run on a SGI Origin 3000 parallel computer using 48 processors at a time. Each of the solutions required about 10GB of memory and a total of about 2500 CPU hours (48 processors x 54 hours) each. For each run, a stringent convergence criterion was used, whereby the solutions were run until changes in the integrated lift coefficient was less than 1.0E-06 per iteration i.e. a change of less than 0.0005 over 500 iterations. Another convergence criterion used was no noticeable change in surface Cp distribution at selected span stations on the wing of the aircraft over 500 iterations. For the most part, these two criteria amounted to a reduction in global flow residuals (L_2 norm) of about 5 orders of magnitude, and required between 3,000 and 10,000 iterations, depending upon the flow initialization and the extent of flow separation.

In Figure 2, computed values of the integrated lift, drag and pitching moment are compared with the experimental data from the two wind-tunnel tests. Not only do the lift coefficient, $C_{L,}$ and the pitching moment coefficient, $C_{m,}$ compare well with the experimental data, the drag coefficient, $C_{D,}$ also matches well which is normally difficult to compute accurately.

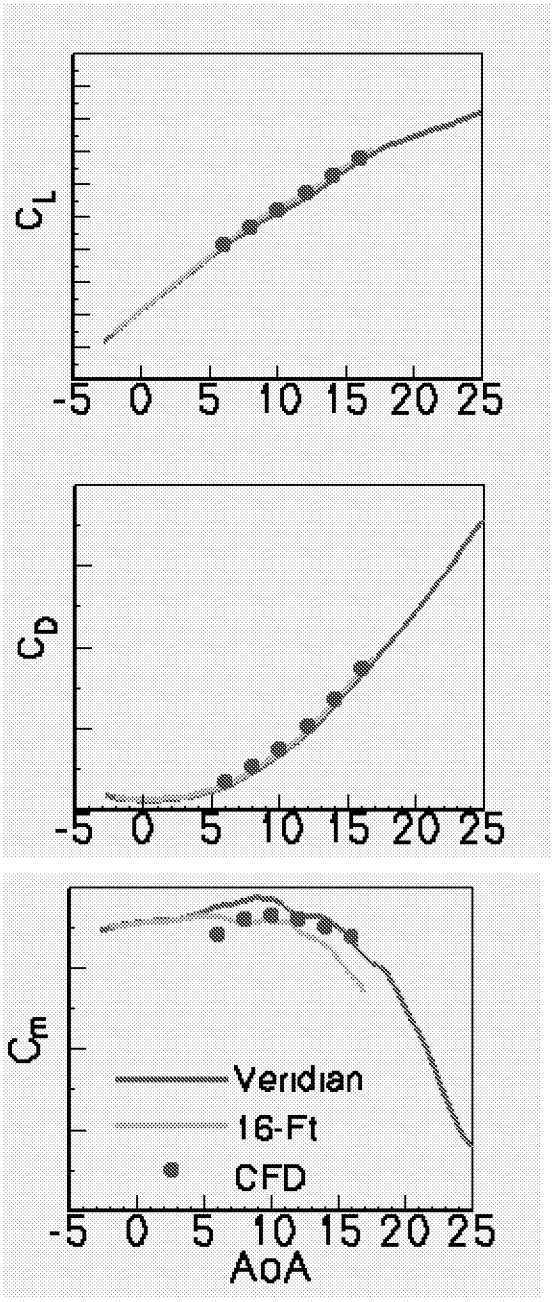

Figure 2: CFD-Experiment comparison for F-16C (Block 25) configuration.

This excellent agreement testifies to the accuracy of the computational method including the adequacy of the grid, the turbulence model and the convergence

criteria used. It may be noted that the experimental data from the two tunnels match closely although both were obtained at slightly different Reynolds numbers. This not only shows the repeatability of the experiments but also a negligible effect of Reynolds number over this small range.

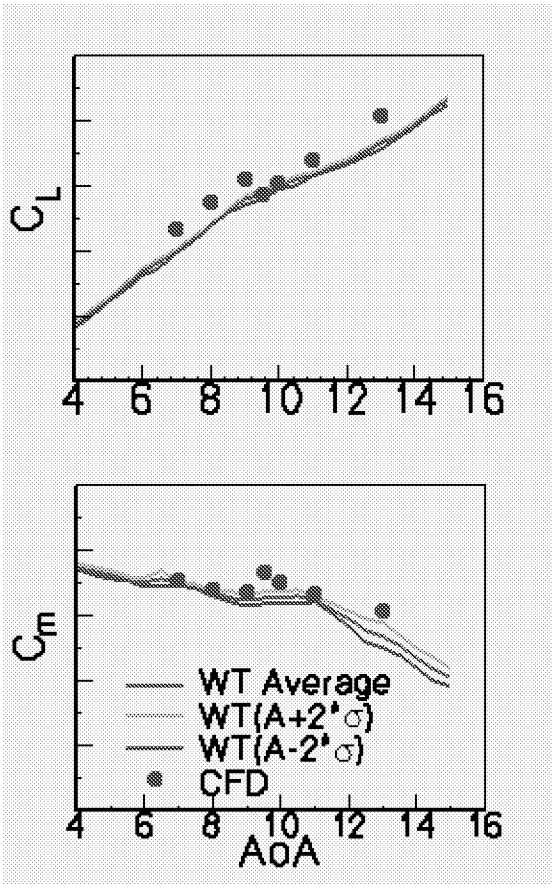

Figure 3: CFD-Experiment Comparison, F/A-18E, 10/10/5 Configuration at M = 0.9, Re/Ft = 3.8 M.

As a further calibration of the code, the CFD data for the F/A-18E configuration are compared against the wind-tunnel Test 523 data from the NASA Langley's 16-FT transonic tunnel. Details of this test can be found in References 6 and 7. As reported in these references, the model experienced severe vibrations at transonic conditions believed to be due to the unsteady movement of shocks on the upper surface of the wing. Because of the unsteady nature of the flow and also as a good wind-tunnel test practice, several repeat runs were made for the transonic conditions in order to obtain an "average" condition during these runs. The comparisons in Figure 3 and 4, show steady-state CFD data plotted against an average of the wind-tunnel test data. In addition, the unsteadiness of the experimental data is quantified by superimposing a ± two times the standard deviation ($\pm 2*\sigma$) at each AoA. In Figure 3 the C_L and C_m are compared for a free stream Mach number of 0.9. Both compare reasonably well except that the CFD shows a sharper break in both C_L and C_m at $\alpha = 9.5^0$ and that the predicted lift is slightly higher. Although the vertical scale is not shown on these plots due to proprietary reasons, the discrepancy in C_L is less than 10%. These slight discrepancies were further evaluated using a finer grid which showed no improvement.

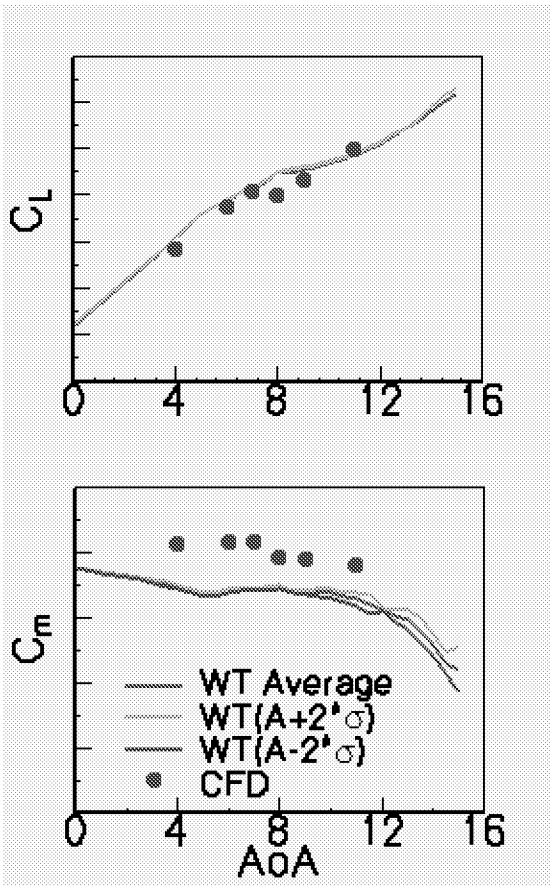

Figure 4: CFD-Experiment Comparison, F/A-18E, 10/10/5 Configuration at Mach = 0.8, Re/Ft=3.8M.

Similar comparisons made for Mach =0.8, in Figure 4, show that while the agreement with the lift coefficient is much better, the predicted C_m is higher. A number of alternative studies, including a grid refinement and use of a different flow solver, were conducted to understand the discrepancy in C_m, but did not show much improvement. A companion study reported in Reference 8 shows improved comparison by using a SST turbulence model with the COBALT flow solver. USM3Dns at this time, however, does not have a tested SST model in the code and hence the stated discrepancy could not be examined further.

ANALYSIS OF COMPUTATIONAL RESULTS

The main aim of the present work is to understand the difference in flow physics between the two configurations studied. It is known, from an analysis of some historical data[8] as well as from wind-tunnel studies conducted during this program, that AWS is a result of one of the wings of an aircraft experiencing a sudden loss of lift resulting from a sudden movement of separation caused by a small change in the angle - of-attack. Thus, an AWS event is characterized by a sudden change in the lift curve slope. The CFD results presented in the earlier section show such a behavior for the pre-production F/A-18E configuration at AoA=9.5 and 8.0 degrees for free-stream Mach numbers of 0.9 and 0.8, respectively. In contrast, the F-16C results shown in Figure 2 display a smooth, almost linear variation. It is, therefore, implied that important Figures of Merit characterizing AWS can be developed by studying the differences in the simulated physical phenomena associated with these two aircraft.

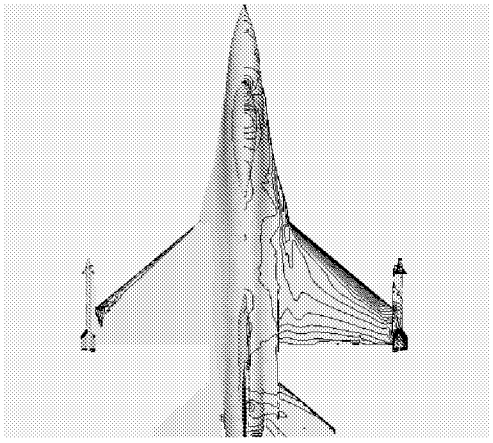

a) $\alpha = 6.0^0$

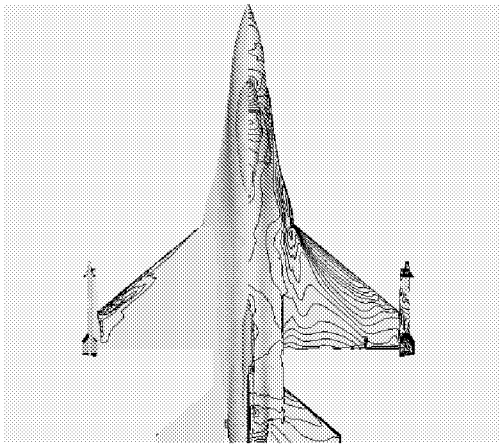

b)$\alpha = 8.0^0$

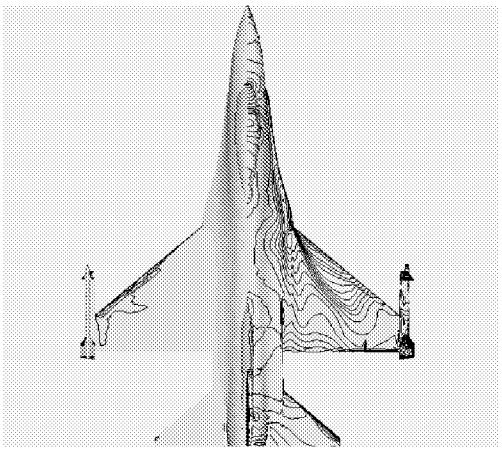

c) $\alpha = 10.0^0$

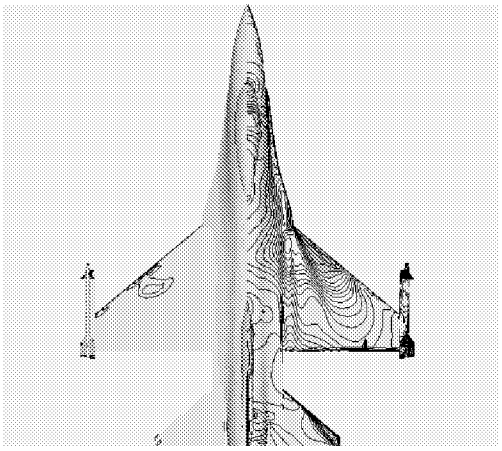

d) $\alpha = 12.0^0$

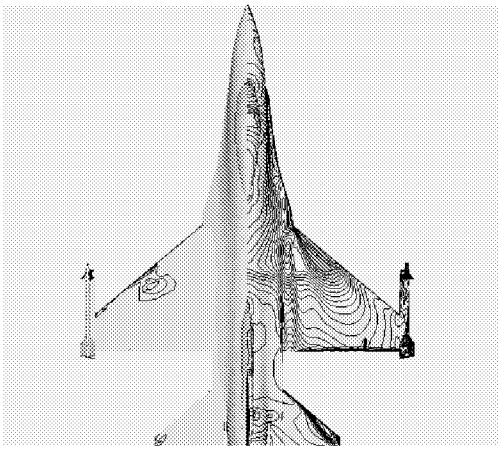

e) $\alpha = 14.0^0$

Figure 5: Cp distribution and separation progression on the wing upper surface for F-16C at M=0.8.

In light of these observations, the CFD results are analyzed for the wing upper surface Cp distribution and the behavior of flow separation as the angle-of-attack is increased for a fixed free-stream Mach number. Figure 5 shows a collage of such plots, one for each AoA, for the benign F-16C configuration. For each frame, the right side shows the surface Cp distribution while on the left side surface contours of negative stream-wise velocity are displayed, the extent of which represents flow separation on the surface.

For lower angles-of-attack only a narrow portion near the wing leading edge shows flow separation. As the angle-of-attack increases, the separation region slowly spreads further downstream but the lift on the configuration keeps increasing in part due to an increased contribution from a stronger Leading Edge Extension (LEX) vortex

A similar collage is shown in Figure 6 for the F/A-18E configuration at a free-stream Mach number of 0.8. Unlike the F-16C, here even at lower angles, there is a strong shock present near the outboard portion of the wing resulting in a small region of boundary layer separation as shown on the left part of the Figure 6a. As the angle-of-attack increases, the shock moves forward, along with an increase in the separated region from downstream of the shock extending all the way to the wing trailing edge. Observe that this behavior suddenly changes as the angle-of-attack is increased from 7.0 to 8.0 degrees where the separation region abruptly spreads from about 30% of the chord all the way to the leading edge of the wing. This sudden change in the separation behavior is associated with a sudden drop in the overall lift for the wing. If this happens asymmetrically, the aircraft may experience a large rolling moment and hence AWS.

In summary, the abrupt change in the extent of separation on the wing upper surface resulting from a small change in angle-of-attack can be indicative of AWS on a configuration.

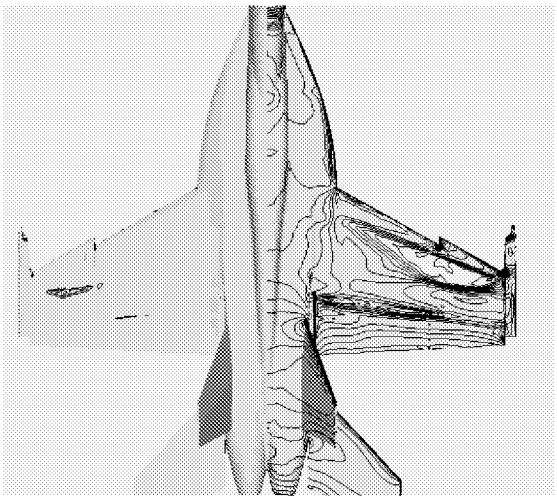

a) $\alpha = 4.0^0$

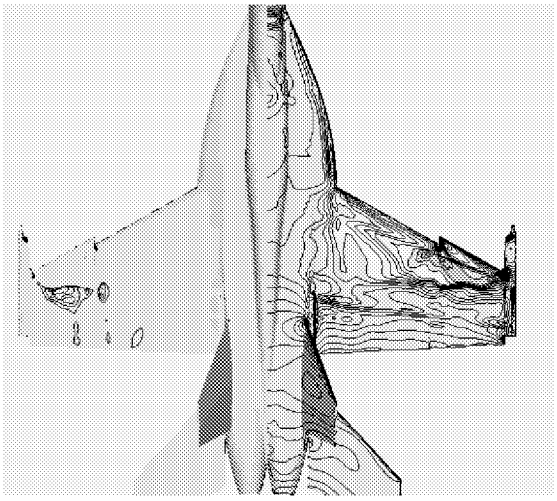

b) $\alpha = 6.0^0$

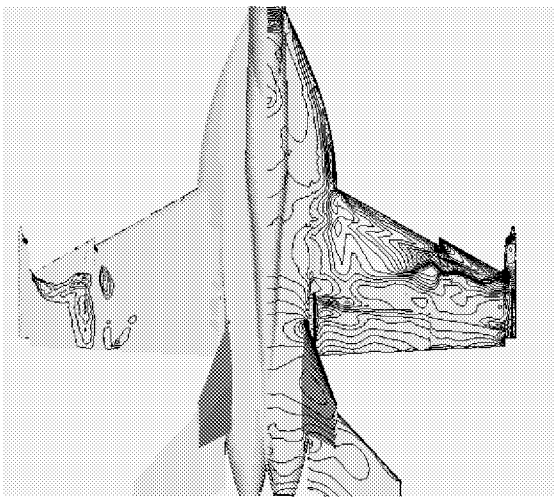

c) $\alpha = 7.0^0$

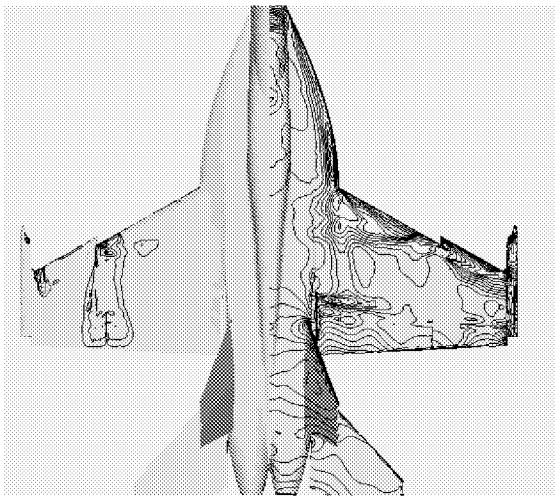

d) $\alpha = 8.0^0$

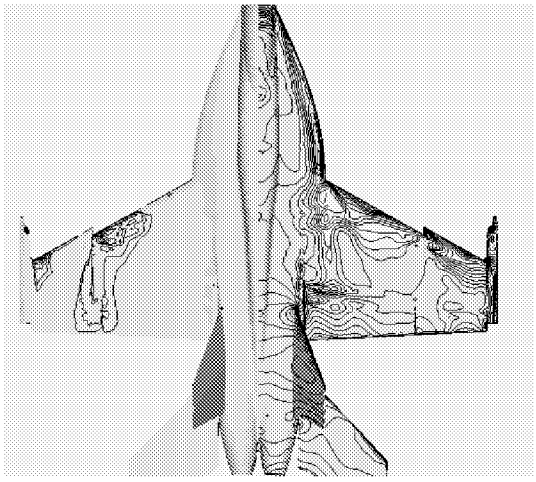

e) $\alpha = 9.0^0$

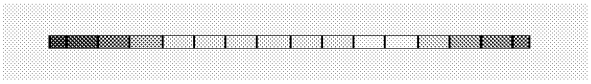

Figure 6: Cp distribution on the wing upper surface for F/A-18E, 10/10/5 at M=0.8.

The steady-state computational results were further analyzed to arrive at aerodynamic indicators against which to measure future configurations for the presence of AWS. As shown for the F/A-18E aircraft, such indicators have to be related to changes in the separation pattern on the lifting wing. Local separation anywhere on a wing should result in a corresponding decrease in lift contribution of that wing panel to the overall lift. Thus, a study of the span-wise distribution of sectional lift can be an indicator of AWS susceptibility. In addition, depending upon the distance of the separated region from the aircraft center line, there will a corresponding decrease in that wing panel's contribution to the total rolling moment of the aircraft. Traditionally, wind-tunnel experiments are conducted on full aircraft configurations. Thus, the rolling moment measured during a wind-tunnel test has contribution of opposite sign from the left and the right wings. Hence the effect of separation on only one of the wings is harder to quantify by measuring the rolling moment. As an alternative, the wind-tunnel programs use wing root bending moment (WRBM) measured by one or more gauges located near the wing root to quantify the effect of separation on the wing.

Based on these considerations, two aerodynamic indicators or Figures of Merit have been proposed and are tested in this study; 1) the span-wise distribution of the wing sectional lift coefficient and its rate of change with respect to α, and 2) the change in the wing root bending moment as AoA changes.

Span-wise distribution of Sectional Lift:

The sectional lift coefficient is defined as the integrated value of the upper and lower surface Cp distribution at a wing span station, where Cp is obtained from the CFD solution.

$$c_l = \int_0^1 \Delta Cp \; d(x/c)$$

The span-wise variation is then obtained by calculating the above integral at several span-wise locations. Such a distribution is shown in Figures 7 and 8 for F-16C and F/A-18E, respectively.

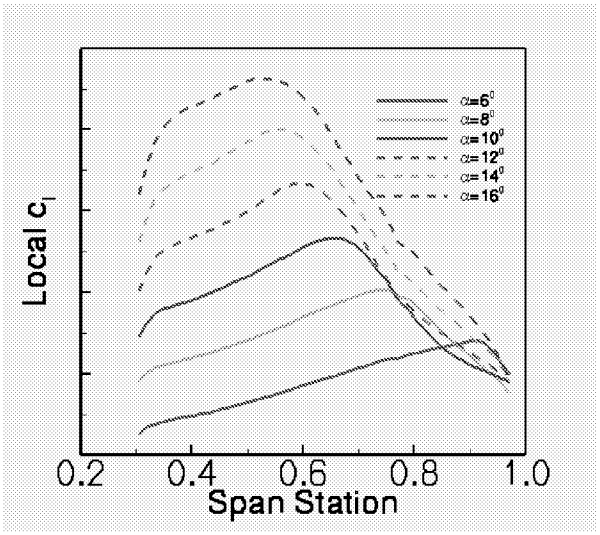

Figure 7: Span-wise distribution of Sectional c_l for F-16C (Block 25) configuration at Mach=0.8.

As shown in Figure 7 for the F-16C configuration, with an increase in the angle-of-attack the lift contribution of the inboard wing panel continues to increase, while that of the outer panel either decreases or remains constant because of the spread of the upper surface separation. But the overall lift increases in a smooth fashion. On the other hand, for the F/A-18E configuration as shown in Figure 8, the span-wise lift distribution that changes dramatically between α=7.0° and 8.0° due to the sudden movement of separation all the way to the wing leading edge signifying an AWS event.

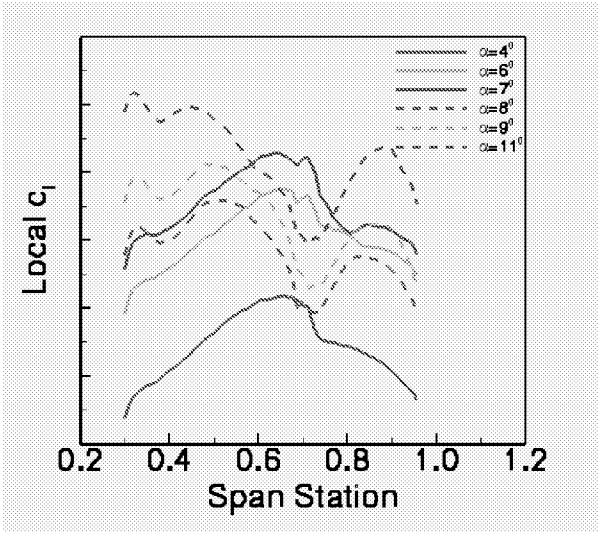

Figure 8: Span-wise distribution of Sectional c_l for F/A-18E, 10/10/5 configuration at Mach=0.8.

Contrasting figure 8 versus figure 7, it is obvious that span-wise distribution of sectional lift distribution across the wing through the stall process can give a quick glance at how abrupt or smooth, the stall process is and may form an important FOM which can be easily evaluated.

Rate of Change of Sectional Lift:

Although the span-wise distribution of sectional c_l can give an indication of AWS, a more definitive insight can be gained by examining its quantitative rate of change with respect to AoA. Figures 9 and 10 show $dc_l/d\alpha$ plotted against the span-station for the F-16C and F/A-18E, respectively. Although the vertical scale is not shown, both figures have been plotted using the same vertical scale, and thus show the relative "strength" or abruptness of the wing stall. As shown in Figure 9 for the F-16C, there is a smooth variation of $dc_l/d\alpha$ across the span, while for the F/A-18E, the large "dip" in Figure 10 around span-station 70%, for the curve labeled α =7.5° corresponds to the AWS phenomenon observed as the AoA changes from 7.0 to 8.0 (ref. Figure 4).

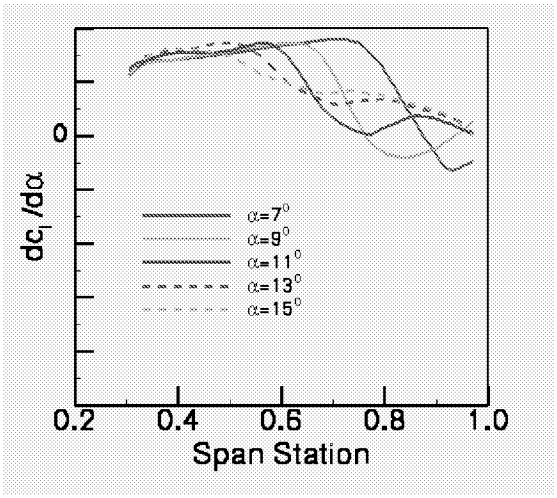

Figure 9: Span-wise distribution of $dc_l/d\alpha$ for F-16C (Block 25) configuration at Mach=0.8.

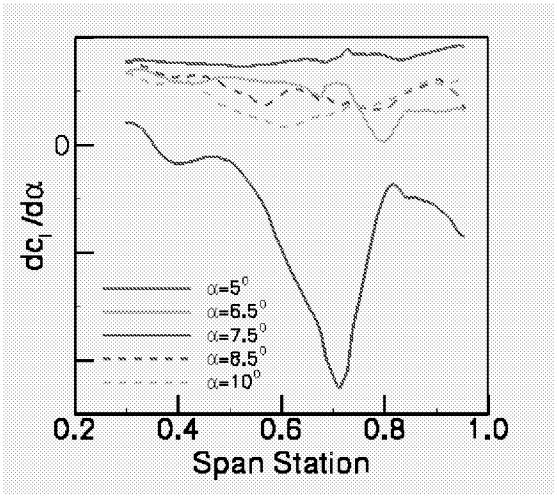

Figure 10: Span-wise distribution of $dc_l/d\alpha$ for F/A-18E, 10/10/5 configuration at Mach=0.8.

Compared to the span-wise distribution of sectional lift, the additional information that plots in Figures 9 and 10 provide is the span-wise location where largest lift loss occurs. Thus, giving the location where design modification efforts need to be concentrated to alleviate AWS.

Wing Root Bending Moment:

Loss of local lift due to flow separation causes corresponding loss of rolling moment (or roll damping), as explained earlier. Based on correlations with wind tunnel and flight test data, it has been shown that abrupt wing stall can occur when the slope

of the WRBM versus AoA curve changes sign[9]. Thus, a study of the WRBM may be used as a potential FOM. This is shown in Figure 11 where the WRBM extracted from the CFD solutions is plotted against the AoA for the two aircraft configurations studied here. The change in the slope between AoA = 7.0^0 and 8.0^0 for the F/A-18E clearly shows the AWS event. It may be noted that all the data on in this figure is CFD data; symbols are shown only for clarity.

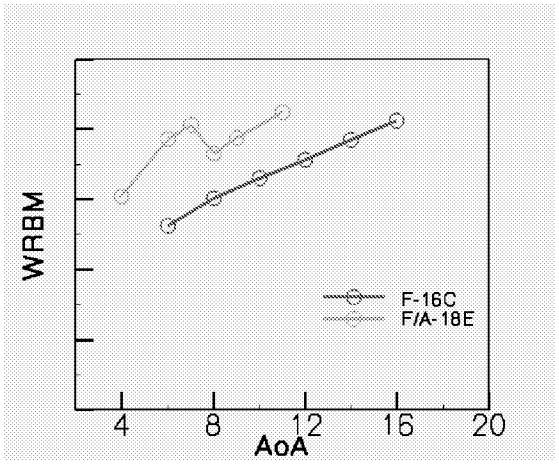

Figure 11: Comparison of wing root bending moment. M = 0.8. All CFD data.

Half-Plane Rolling Moment:

While calculation of WRBM from CFD studies is straight forward, it does involve additional computations of force integration not normally done as part of a routine CFD calculation. Since normally a CFD study is performed on only half of a symmetrical configuration to save computational resources, and since the rolling moment calculated for ½ of the configuration (termed Half-Plane Rolling Moment, HPRM) is a routine output for most CFD computations, it can be used, instead of WRBM, as a potential FOM. This is shown in Figure 12 where HPRM is compared for the two configurations. The similarity of the curves in Figures 11 and 12, thus establishes HPRM from ½ configuration CFD analyses as a viable FOM for any AWS study.

In addition, as has been shown in Part II of this study (Ref. 1), at times the HPRM versus AoA curve is a little clearer indicator of the wing stall compared to a lift curve.

In summary, as shown above, the potential FOMs for any abrupt wing stall study using steady CFD are:

1. The span-wise variation of sectional lift and its rate of change with respect to AoA, and
2. The slope change in the C_L, WRBM (or equivalently HPRM) versus the AoA.

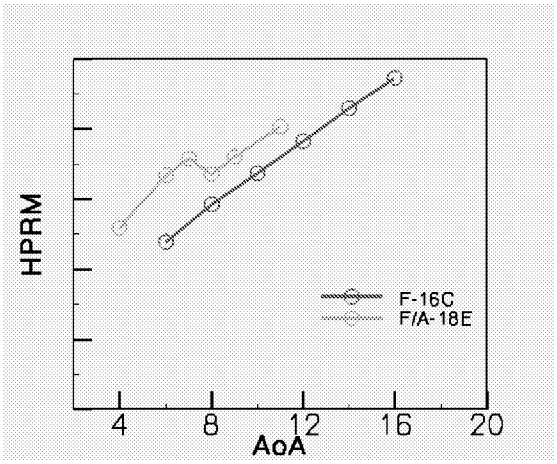

Figure 12: Comparison of half-plane rolling moment. M = 0.8. All CFD data.

CONCLUSIONS

A validated CFD procedure based on an unstructured grid method and steady state Navier-Stokes solutions has been developed for evaluating AWS behavior of aircraft. A set of Figures of Merit have been developed by analyzing CFD results on configurations that do and do not show AWS tendencies. The static FOMs include slope change in the C_L and WRBM versus AoA curve as well as a sudden change in the span-wise distribution of local lift. In addition, the half-plane rolling moment (HPRM) calculated from ½ configuration CFD is shown to provide the same information in predicting AWS as the WRBM, thus establishing HPRM as a viable FOM for steady state CFD studies.

Results of these and other companion CFD studies conducted under the AWS program have been used to prepare CFD based recommendations[10] that may be used to evaluate future configurations for AWS susceptibility or lack their of.

ACKNOWLEDGEMENTS

This work was supported by the NASA Aerospace Systems Concepts to Test (ASCoT) program, NAVAIR, and the Office of Naval Research. The authors would like to thank Dr. Edward Parlette of Vigyan, Inc. for grid generation help and to Mr. Jonathan Nehrbass, a co-op student in the Configuration Aerodynamics Branch at NASA Langley, for graphics related help.

REFERENCES

1. Chung, J., and Parikh, P., "A Computational Study of the Abrupt Wing Stall (AWS) Characteristics for various Fighter Jets: Part II, AV-8B and F/A-18C", AIAA-2003-0747, January 2003.

2. Frink, N.T., Pirzadeh, S., Parikh, P., Pandya, M.J., and Bhat, M.K., "The NASA Tetrahedral Unstructured Software System (TetrUSS)", ***The Aeronautical Journal***, Vol. 104, No. 1040, October 2000, pp. 491-499.

3. Pirzadeh, S., "Three-Dimensional Unstructured Viscous Grids by the Advancing Layers Method", ***AIAA Journal***, Vol. 34, No. 1, January 1996, pp. 43-49.

4. Frink, N.T., "Tetrahedral Unstructured Navier-Stokes Method for Turbulent Flows", ***AIAA Journal***, Vol. 36, No. 11, November 1998, pp. 1975-1982.

5. Bhat, M. K. and Parikh, P., "Parallel Implementation of an Unstructured Grid-Based Navier-Stokes Solver", AIAA Paper 99-0663, January 1999.

6. McMillin, N., Hall, R. and Lamar, J., "Understanding Abrupt Wing Stall with Experimental Methods (Invited)", AIAA-2003-0591, January 2003.

7. Schuster, D. and Byrd, J., "Transonic Unsteady Aerodynamics of the F/A-18E at Conditions Promoting Abrupt Wing Stall (Invited)", AIAA-2003-0593, January 2003.

8. Forsythe, J. R. and Woodson, S.H., "Unsteady CFD Calculations of Abrupt Wing Stall Using Detached-Eddy Simulation", AIAA-2003-0594, January 2003.

9. Green, B.E. and Ott, J.D., "F/A-18C to E Wing Morphing Study for the Abrupt Wing Stall Program", AIAA-2003-0925, January 2003.

10. Woodson, S., et al, "Recommendations for CFD Procedures for Predicting Abrupt Wing Stall (AWS) (Invited)", AIAA-2003-0923, January 2003.